Journal of Electroceramics (2018) 40:306–315
https://doi.org/10.1007/s10832-018-0131-4

Temperature-dependence of electrical properties for the ceramic composites based on potassium polytitanates of different chemical composition

N. V. Gorshkov[1] · V. G. Goffman[1] · M. A. Vikulova[1] · D. S. Kovaleva[1] · E. V. Tretyachenko[1] · A. V. Gorokhovsky[1]

Received: 11 August 2017 / Accepted: 9 March 2018 / Published online: 23 March 2018
© Springer Science+Business Media, LLC, part of Springer Nature 2018

Abstract
The samples of ceramic materials based on potassium polytitanate (PPT) characterized with various TiO_2/K_2O molar ratio, are produced by calcination at 900 °C and investigated. AC conductivity (σ_{ac}) of the obtained ceramics is measured at different temperatures between 200 and 800 °C in frequency range of 0.1 Hz–1 MHz. The method of combined impedance and modulus spectroscopy is used to analyze the obtained results. The activation energies of DC conductivity, bulk and grain-boundary conductivity as well as relaxation frequency for studied composites are estimated. Using the correlated barrier hopping (CBH) model, the energies of potential barrier between neighboring defect sites for all kinds of investigated materials are presented. The bulk and grain boundary parameters of the produced ceramic materials based on potassium polytitanates are calculated. The mechanism of different vacancies formation in the investigated ceramic system is discussed. The influence of precursor chemical composition on electrical properties for the ceramic composites based on potassium polytitanates is studied.

Keywords Multiphase ceramics · Impedance spectroscopy · Electric conductivity · Relaxation processes · Oxygen vacancies · Grain boundary

1 Introduction

Ceramic materials, including titanates, with mixed ionic-electronic conductivity can be applied in different areas of science and technology, namely semiconductors, electrochemical energy storage materials, electrodes of fuel cells and batteries, separation membranes and catalysts [1]. It is known that alkali and alkaline earth niobates and titanates, are considered as promising alternative ceramic materials because of excellent electric characteristics at high temperatures [2–4]. Besides, such layered materials are well polarized and environmentally friendly. It is known that alkalis can be easy volatized at high temperatures and this process promotes formation of oxygen vacancies supporting increased electrical conductivity [1]. Depending the desired electrical properties of the ceramic material obtained in alkali titanate or alkali niobate systems, this effect may be considered as positive or negative phenomenon. That is why an investigation of electrical properties of the ceramic composites containing alkali titanates taking into account both (ionic and electronic) kinds of conductivity at different frequencies is of a high interest. The outcomes of some previous research related to the investigation of electrical properties of alkali titanates ($Na_2Ti_3O_7$, $NaKTi_3O_7$, $K_2Ti_4O_9$), [5, 6] indicates their specific features and potential application as multifunctional ceramic materials.

In this research, the alkali titanate ceramics were produced using amorphous potassium polytitanate (PPT) as raw material. PPT is characterized by chemical formula of $K_2O{\cdot}nTiO_2{\cdot}mH_2O$, where n can vary from 2 to 6 and m changes from 0.5 to 2.0 depending on the synthesis conditions. Generally, different kinds of PPT are produced by the treatment of TiO_2 powder in the molten mixtures of KOH-KNO_3 system at 450–550 °C [7]. The obtained PPT particles have layered structure similar to other kinds of crystalline potassium titanates and formed by polyanion sheets consisting of TiO_6 octahedra; whereas their interlayer space is filled with cations of K^+ and/or H_3O^+ [7–10] as well as contains H_2O molecules. It has been shown [11, 12] that at room temperature the activation energy of relaxation processes (E_a) taking place in PPT is varied in the range of 0.07–0.19 eV, and protons were the main charge carriers at these conditions. It was

✉ N. V. Gorshkov
gorshkov.sstu@gmail.com

[1] Yuri Gagarin State Technical University of Saratov, Saratov, Russian Federation

also recognized [13] that high-temperature treatment (calcination) of the PPT compacts promoted obtaining the multiphase ceramic materials consisting of the mixture of tetra-, hexa- and octatitanate crystalline phases characterized with high ion conductivity and permittivity ($\varepsilon = 10^2$–10^5 depending on frequency). Thus, the goal of this work is to study the frequency and temperature dependences of AC and DC conductivity for the ceramic composites obtained by calcination of the compacted potassium polytitanates of different chemical composition at 900 °C.

2 Experimental

Potassium polytitanate powder was synthesized by molten salt method earlier described in [7] using TiO_2 (30 wt.%), KOH (30 wt.%) and KNO_3 (40 wt.%) as raw materials. The batch of powdered raw materials (100 g) was mixed with 60 ml of distilled H_2O; the obtained dispersion was agitated to dissolve KOH and KNO_3 and further thermally treated at 500 °C for 2 h in the electrical furnace. The obtained parent product was treated using H_2SO_4 solution until obtaining stable pH values of the dispersions equal to 7.5, 9.2 or 10.1 (hereinafter referred as PPT(7.5), PPT(9.2) and PPT(10.1), and further carefully washed with distilled water and dried at 50 °C for 4 h. The synthesized PPT powders consisted of amorphous flakes (100–800 nm in diameter, 10–20 nm of thickness) partially aggregated in spherical agglomerates of 1.5–3.0 μm in diameter similar to the products described in [13].

Further, the samples of the powdered products were compacted at 200 MPa to produce the tablets of 12 mm in diameter and 2.0 ± 0.1 mm in thickness, heated at 900 °C for 4 h and grinded using vibratory micro mill Pulverisette 0 Fritsch (Germany). The abovementioned cycle of operations was repeated three times until stable phase composition and homogeneous structure of particles were obtained. The phase composition of the obtained ceramic powders was analyzed by XRD (ARL X'TRA. Switzerland). Morphology of the PPT particles and structural features of the obtained ceramics were studied by SEM method using Scanning Electron Microscope EXplorer ASPEX (USA).

The chemical composition of the produced ceramic materials is found by WDX method (Spectroscan MAX-GV, Russia) and reported in Table 1.

After the final heating the bases of the produced ceramic discs were covered by silver-palladium adhesive (K13 trade mark, Russia) and studied by impedance spectroscopy using an impedance analyzer (Novocontrol Alpha AN, Germany) at different temperatures in the range of 200–800 °C at the frequencies varied in the range of 0.1 Hz – 1 MHz with amplitude of 100 mV.

Table 1 Chemical composition of the potassium polytitanates treated at different pH

pH	Characteristics					
	Oxides content, wt.%					TiO_2/K_2O molar ratio
	TiO_2	SO_3	K_2O	Al_2O_3	SiO_2	
7.5	91.0	0.2	7.8	0.5	0.5	11.7
9.2	87.0	0.1	12.2	0.6	0.2	7.1
10.1	83.0	0.4	15.8	0.4	0.5	5.3

3 Results

3.1 Structure and microstructural studies

The XRD patterns of the ceramics produced using different kinds of PPT are reported in Fig. 1.

All the obtained ceramic materials are represented as multiphase systems. The composite based on PPT-7.5 contained $K_3Ti_8O_{17}$ as well as TiO_2 in the forms of anatase and rutile. The phase composition of the ceramics based on PPT-9.2 represents two main crystalline phases, namely $K_2Ti_4O_9$ and $K_3Ti_8O_{17}$. At the same time, the ceramic composite obtained with PPT-10.1 consisted of $K_3Ti_8O_{17}$ crystalline phase only. Taking into account that the XRD reflections of $K_3Ti_8O_{17}$ are more intensive in all the ceramic materials produced; this phase, characterized with rod-like crystalline structure, can be considered as a dominant component of the investigated ceramic materials.

The structure of the obtained ceramic materials is illustrated in Fig. 2.

The crystals of the composite based on PPT-7.5 have quasi-spherical (TiO_2), platy ($K_2Ti_4O_9$) and rod-like ($K_3Ti_8O_{17}$) morphology in a good agreement with the XRD data (Fig.

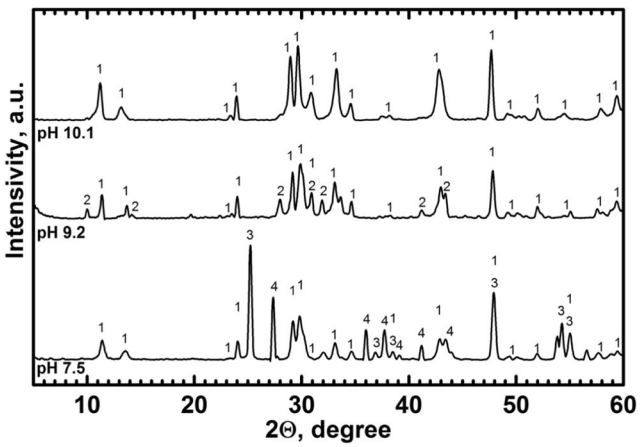

Fig. 1 XRD patterns of PPT based ceramics of different chemical composition obtained at 900 °C for 4 h: 1 - [010–72-1699] $K_3Ti_8O_{17}$; 2 - [000–32-0861] $K_2Ti_4O_9$, 3 – [010–75-2544] TiO_2 (Anatase), 4 – [010–72-7374] TiO_2 (Rutile)

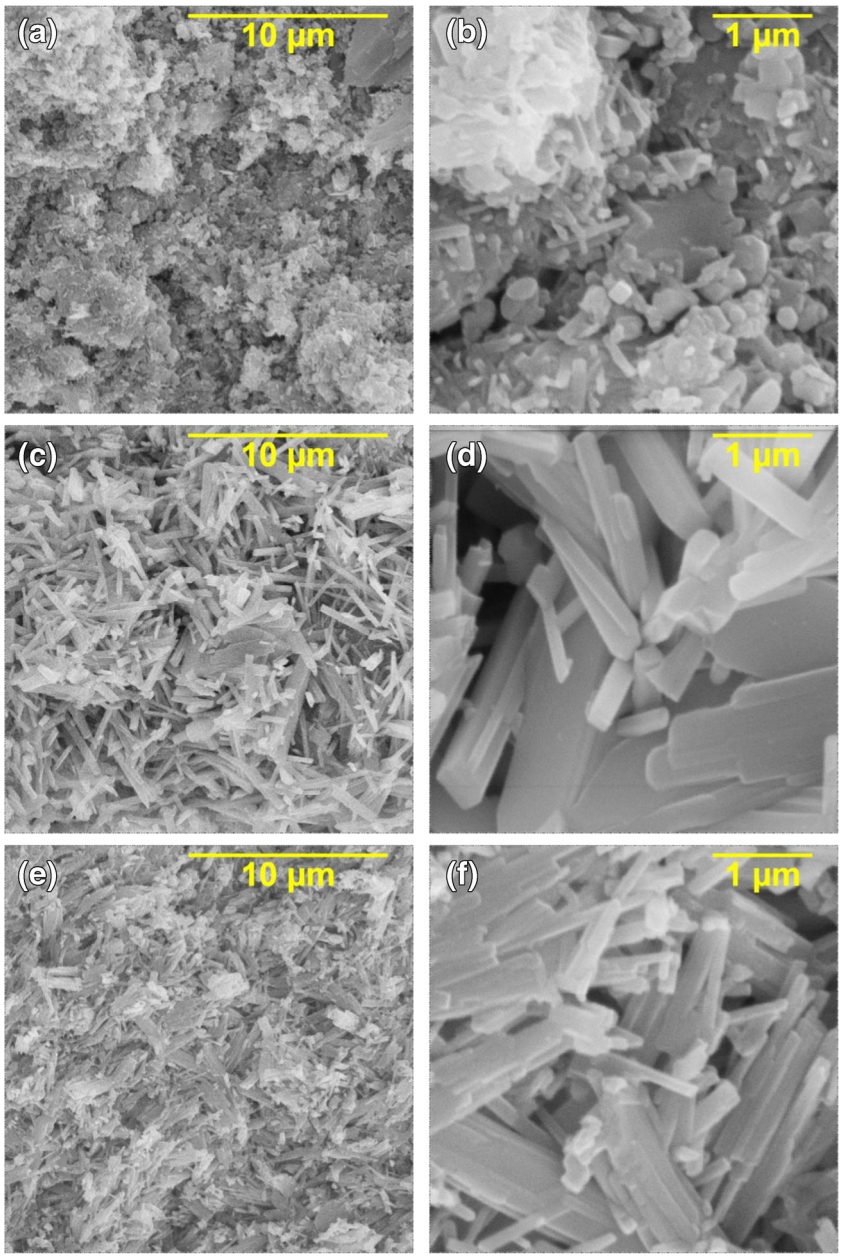

Fig. 2 Micrographs (SEM) of the obtained ceramic composites (fracture surfaces) based on different potassium polytitanates: PPT-7.5 (**a** and **b**), PPT-9.2 (**c** and **d**) and PPT-10.1 (**e** and **f**)

2a, b). The structure of ceramic body produced with PPT-9.2 powder is formed by rod-like crystals; the diameter of rods varies in the range of 0.1–0.8 μm, whereas the length is of 2–3 μm. An average aspect-ratio (AR) of these crystals is not so big (AR = 6–10), whereas $K_2Ti_4O_9$ and $K_3Ti_8O_{17}$ whiskers usually are characterized with AR = 30–60 [14, 15]. Such shape of the crystals corresponds to the XRD data (Fig. 1), where reduced intensities of the reflections in low-angle range of 2Θ are recognized. In addition, some inclusions of $K_2Ti_4O_9$ crystals having platy shape can be recognized in the microphotographs (Fig. 2c, d); whereas, both crystals can be presented as rods of different diameter [16]. The composites based on PPT-10.1 generally consist of rod-like crystals of $K_3Ti_8O_{17}$ with AR = 30–60.

The analysis of XRD patterns indicates a presence of some quantity of the amorphous phase in all the materials produced (in mol. %): 12.9 (PPT-7.5), 17.6 (PPT-9.2) and 9.3 (PPT-10.1). The general chemical composition of the PPT-9.2 system corresponds to the molar ratio of $[TiO_2]_0/[K_2O]_0 = 7.1$; whereas, the crystalline phases (CP) appeared in the ceramic body by sintering at 900 °C are characterized with $[TiO_2]_{CP}/[K_2O]_{CP} = 4$ ($K_2Ti_4O_9$) or 5.3 ($K_3Ti_8O_{17}$). Thus, it is possible to assume that the residual amorphous phase (AP) appeared in this system at 900 °C has $[TiO_2]_{AP}/[K_2O]_{AP} > 7.1$ due to accumulating of the potassium oxide in the crystalline phases.

3.2 Electrical conductivity

Complex impedance spectroscopy is used to study the electrical behavior of composites based on potassium polytitanates treated at different pH. All the measurements were made in the range of 200–800 °C with a step of 50 degrees at 0.1 Hz – 1 MHz and analyzed using the following formulas:

$$Z^{\wedge} = \frac{R}{2}, \tag{1}$$

$$M^{\wedge} = \frac{C_0}{2 \cdot C}, C_0 = \frac{\varepsilon_0 \cdot \varepsilon \cdot S}{d}, \tag{2}$$

$$2 \cdot \pi \cdot f \cdot R \cdot C = 1, \tag{3}$$

where

Z”	the imaginary part of impedance
R	resistance
M”	the imaginary part of electric modulus
C	capacity
ε_0	the permittivity of free space
ε	the permittivity of material
S	the area of electrode
d	the sample thickness
f	frequency.

The sample of typical variation of the imaginary part of impedance (Z”) and modulus (M”) with frequency is reported in Fig. 3 for the composite based on PPT-7.5 (T = 400 °C). The Cole-Cole plot of this composite and equivalent circuit of the impedance data are shown in Fig. 4.

The peak height of Z" peak is proportional to R and the peak height of M" peak is proportional to C^{-1}. On the other hand, the frequency of the Z” and M” maxima depends on electric resistance and capacitance, according to the relations marked in Fig. 3. The values of f_{max} of Z” and M” peaks as well as bulk and grain boundary parameters at different

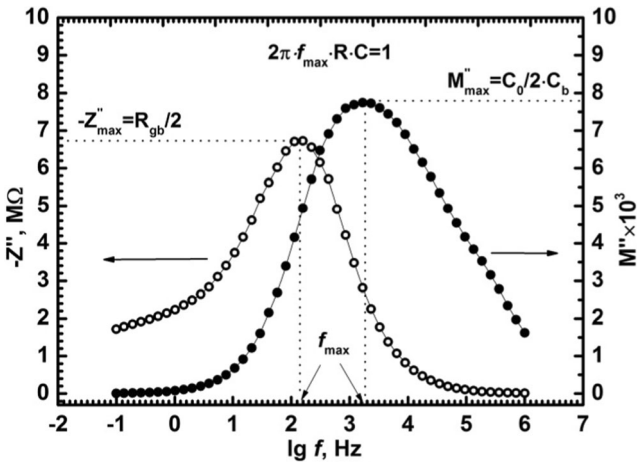

Fig. 3 The spectroscopic plots of imaginary part of impedance (Z”) and modulus (M”) for the PPT-7.5 based ceramic composite (T = 400 °C)

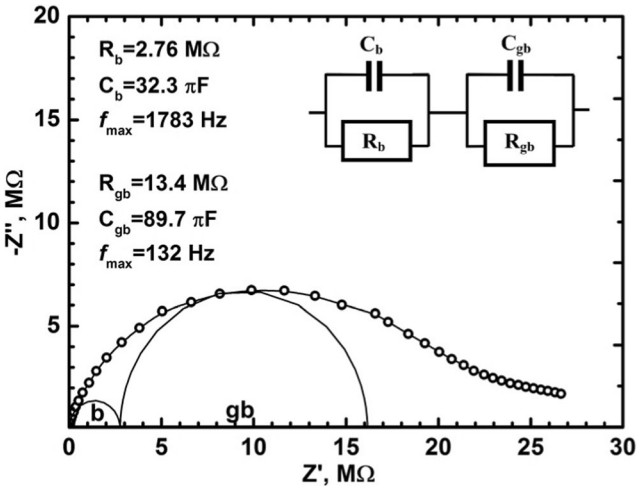

Fig. 4 The Cole-Cole plot and equivalent circuit of the impedance data for the PPT-7.5 based ceramic composite (T = 400 °C)

temperatures calculated in the same manner for all the studied materials are shown in Tables 2 and 3.

An influence of frequency on electrical conductivity for the investigated ceramic composites at several temperatures is plotted in Fig. 5. It is observed that σ_{dc} values increase with increasing the temperature.

The obtained experimental data on σ_{ac} frequency dependence are described by the equation [17, 18].

$$\sigma_{ac}(\omega) = \sigma_{dc} + A\omega^s \tag{4}$$

where

σ_{dc}	DC conductivity
A	constant, independent of frequency
ω	angular frequency
s	characteristic parameter.

As seen from the graphs, an increase of the temperature promotes increased values of the high frequency border of frequency independent region (f_b) for all the studied composites. Stable σ_{dc} values obtained for σ_{ac} in the abovementioned regions comply with the Eq. (4). At frequencies corresponding to the range of $f > f_b$, σ_{ac} is proportional to f and conductivity rises rapidly. It is possible to note also that an increase of the temperature promotes more smooth character of $\sigma_{ac}(f)$ curves at $f > f_b$.

The DC conductivity of the produced ceramic composites can be expressed by well-known Arrhenius equation:

$$\sigma_{dc} = \sigma_0 \cdot exp(-E_a/k_B T), \tag{5}$$

where

σ_0	pre-exponential factor
E_a	activation energy of conductivity
k_B	Boltzmann constant
T	temperature.

Table 2 Characteristics of the equivalent circuits based on the impedance data (bulk conductivity) at different temperatures for the composites obtained

T (°C)	Characteristics								
	Composite based on PPT-7.5			Composite based on PPT-9.2			Composite based on PPT-10.1		
	R_b (Ω)	C_b (F)	f_{max} of Z" (Hz)	R_b (Ω)	C_b (F)	f_{max} of Z" (Hz)	R_b (Ω)	C_b (F)	f_{max} of Z" (Hz)
200	$1.30{\cdot}10^{9}$	$3.33{\cdot}10^{-11}$	3.67	$6.99{\cdot}10^{5}$	$3.22{\cdot}10^{-11}$	706	$6.97{\cdot}10^{7}$	$3.71{\cdot}10^{-11}$	61.6
250	$3.06{\cdot}10^{8}$	$3.45{\cdot}10^{-11}$	15.1	$2.36{\cdot}10^{5}$	$3.28{\cdot}10^{-11}$	20,550	$1.16{\cdot}10^{7}$	$3.38{\cdot}10^{-11}$	404
300	$5.79{\cdot}10^{7}$	$3.39{\cdot}10^{-11}$	81	$1.22{\cdot}10^{5}$	$3.42{\cdot}10^{-11}$	38,143	$2.05{\cdot}10^{6}$	$3.19{\cdot}10^{-11}$	2431
350	$9.19{\cdot}10^{6}$	$3.33{\cdot}10^{-11}$	520	$2.33{\cdot}10^{4}$	$3.68{\cdot}10^{-11}$	185,780	$5.71{\cdot}10^{5}$	$2.81{\cdot}10^{-11}$	9914
400	$2.76{\cdot}10^{6}$	$3.23{\cdot}10^{-11}$	1783	$1.78{\cdot}10^{4}$	$3.47{\cdot}10^{-11}$	257,039	$2.10{\cdot}10^{5}$	$2.72{\cdot}10^{-11}$	27,832
450	$1.00{\cdot}10^{6}$	$3.12{\cdot}10^{-11}$	5086	$1.02{\cdot}10^{4}$	$3.07{\cdot}10^{-11}$	510,505	$7.88{\cdot}10^{4}$	$2.59{\cdot}10^{-11}$	77,890
500	$4.04{\cdot}10^{5}$	$3.00{\cdot}10^{-11}$	13,110	$5.55{\cdot}10^{3}$	$2.87{\cdot}10^{-11}$	1,000,000	$3.70{\cdot}10^{4}$	$2.44{\cdot}10^{-11}$	176,717
550	$9.57{\cdot}10^{4}$	$3.09{\cdot}10^{-11}$	53,860	–	–	–	$1.59{\cdot}10^{4}$	$2.35{\cdot}10^{-11}$	426,628
600	$4.45{\cdot}10^{4}$	$2.92{\cdot}10^{-11}$	122,410	–	–	–	$7.19{\cdot}10^{3}$	$2.21{\cdot}10^{-11}$	1,000,000
650	$2.18{\cdot}10^{4}$	$2.79{\cdot}10^{-11}$	260,765	–	–	–	–	–	–
700	$1.13{\cdot}10^{4}$	$2.77{\cdot}10^{-11}$	509,330	–	–	–	–	–	–
750	$5.82{\cdot}10^{3}$	$2.74{\cdot}10^{-11}$	1,000,000	–	–	–	–	–	–

Figure 6 shows Arrhenius plot of DC conductivity, caused by mixed electron-ion conductivity, for the investigated ceramic composites. Two linear regions with different slope can be clearly identified at different temperature ranges, depending on pH treatment. The activation energies of conductivity, calculated for these regions, are given in Table 3.

Obtained experimental data is in a good agreement with the correlated barrier hopping model (CBH) [19]. Wherein, carrier charges of ceramics based on PPT, treated at different pH, move within a defect-potential slit (well) and between the nearest neighbor sites over the potential barrier W_{max}. These processes are called as short-range intrawell hopping (SRIH) and long-range interwell hopping (LRIH) [20]. In CBH model the frequency exponent s is evaluated by equation [21]:

$$s = 1-(6k_BT/W_{max}) \quad (6)$$

W_{max} is found from the linear regions slope on the *(1-s)-T* graphs (Fig. 7) and has values 1.96, 0,64 and 0,97 eV for low temperature range ($T < 400$–500 °C) and 0.36, 0.27 and

Table 3 Characteristics of the equivalent circuits based on the impedance data (grain boundary conductivity) at different temperatures for the composites obtained

T (°C)	Characteristics								
	Composite based on PPT-7.5			Composite based on PPT-9.2			Composite based on PPT-10.1		
	R_{gb} (Ω)	C_{gb} (F)	f_{max} of M" (Hz)	R_{gb} (Ω)	C_{gb} (F)	f_{max} of M" (Hz)	R_{gb} (Ω)	C_{gb} (F)	f_{max} of M" (Hz)
200	$8.16{\cdot}10^{9}$	$1.39{\cdot}10^{-10}$	0.14	$1.88{\cdot}10^{8}$	$1.72{\cdot}10^{-9}$	0.49	$5.66{\cdot}10^{8}$	$7.42{\cdot}10^{-10}$	0.38
250	$1.65{\cdot}10^{9}$	$1.12{\cdot}10^{-10}$	0.86	$3.32{\cdot}10^{7}$	$1.48{\cdot}10^{-9}$	3.25	$1.61{\cdot}10^{8}$	$5.82{\cdot}10^{-10}$	1.69
300	$2.55{\cdot}10^{8}$	$1.09{\cdot}10^{-10}$	5.72	$1.09{\cdot}10^{7}$	$1.34{\cdot}10^{-9}$	10.8	$3.72{\cdot}10^{7}$	$7.61{\cdot}10^{-10}$	5.62
350	$4.83{\cdot}10^{7}$	$9.60{\cdot}10^{-11}$	34	$1.95{\cdot}10^{6}$	$6.08{\cdot}10^{-10}$	134	$7.56{\cdot}10^{6}$	$1.31{\cdot}10^{-9}$	16
400	$1.34{\cdot}10^{7}$	$8.97{\cdot}10^{-11}$	132	$6.72{\cdot}10^{5}$	$1.98{\cdot}10^{-10}$	1194	$2.34{\cdot}10^{6}$	$1.07{\cdot}10^{-9}$	64
450	$4.58{\cdot}10^{6}$	$8.00{\cdot}10^{-11}$	434	$1.31{\cdot}10^{5}$	$1.89{\cdot}10^{-10}$	6427	$6.24{\cdot}10^{5}$	$7.43{\cdot}10^{-10}$	343
500	$1.71{\cdot}10^{6}$	$8.15{\cdot}10^{-11}$	1143	$3.85{\cdot}10^{4}$	$1.73{\cdot}10^{-10}$	23,978	$1.95{\cdot}10^{5}$	$3.51{\cdot}10^{-10}$	2326
550	$4.75{\cdot}10^{5}$	$6.99{\cdot}10^{-11}$	4790	$1.16{\cdot}10^{4}$	$1.29{\cdot}10^{-10}$	106,623	$5.62{\cdot}10^{4}$	$1.61{\cdot}10^{-10}$	17,558
600	$1.90{\cdot}10^{5}$	$6.88{\cdot}10^{-11}$	12,156	$4.54{\cdot}10^{3}$	$1.07{\cdot}10^{-10}$	326,926	$1.87{\cdot}10^{4}$	$9.70{\cdot}10^{-11}$	87,658
650	$7.45{\cdot}10^{4}$	$6.32{\cdot}10^{-11}$	33,816	–	–	–	$7.09{\cdot}10^{3}$	$7.36{\cdot}10^{-11}$	304,796
700	$3.11{\cdot}10^{4}$	$6.09{\cdot}10^{-11}$	84,230	–	–	–	$2.65{\cdot}10^{3}$	$6.01{\cdot}10^{-11}$	1,000,000
750	$1.34{\cdot}10^{4}$	$6.37{\cdot}10^{-11}$	185,780	–	–	–	–	–	–
800	$5.44{\cdot}10^{3}$	$5.73{\cdot}10^{-11}$	510,200	–	–	–	–	–	–

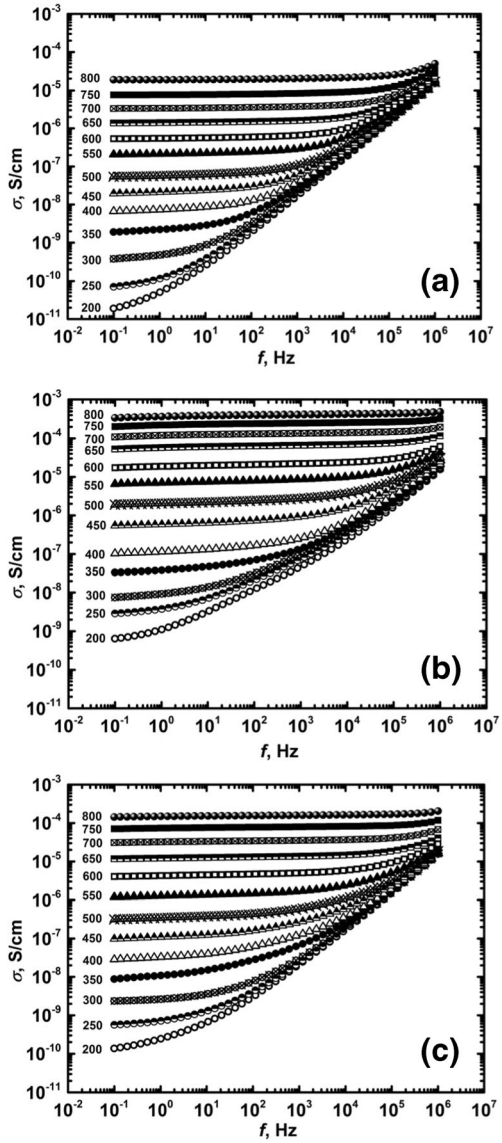

Fig. 5 Frequency dependence of the electrical conductivity for ceramic composites based on PPT-7.5 (**a**), PPT-9.2 (**b**) and PPT-10.1 (**c**), at several temperatures

0.28 eV for high temperature range ($T > 400$–500 °C), depending on chemical composition of the potassium polytitanate (pH of the parent PPT treatment 7.5, 9.2 and 10.1 respectively).

The peak frequency as well as bulk and grain-boundary conductivity can also be represented by the Arrhenius relation (Figs. 8, 9, 10 and 11).

$$f_{max} = f_0 \exp(-E_a/k_B T), \quad (7)$$

where

f_0 pre-exponential factor
E_a activation energy of relaxation frequency
k_B Boltzmann constant
T temperature

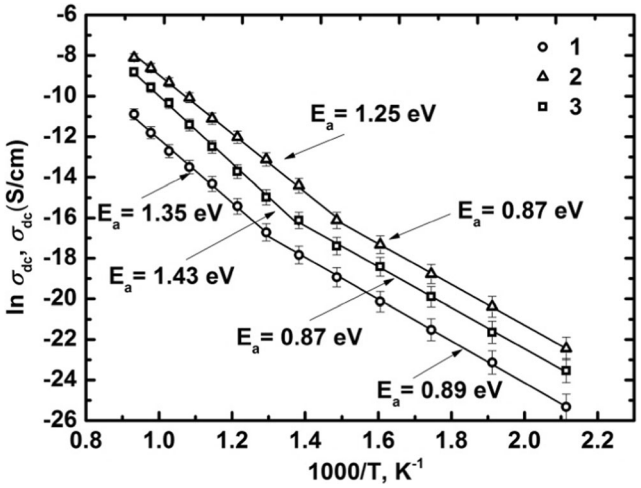

Fig. 6 Arrhenius plot of DC conductivity for ceramic composites based on PPT-7.5 (1), PPT-9.2 (2) and PPT-10.1 (3), at different temperatures

The Arrhenius plots for bulk conductivity and relaxation frequency from M" for all the curves show the linear behavior, but graphs of grain-boundary conductivity and relaxation frequency from Z" relaxation have two linear regions. The data on activation energy calculated for these processes for all the investigated systems in different temperature ranges are presented in Table 4.

4 Discussion

The SEM outcome is in a good agreement with the XRD data. The obtained results correspond to the trends of crystallization of PPT systems recognized earlier [7].

The following dependence between the phase composition of the obtained ceramic composite and the chemical composition of the PPT precursor can be noted (Table 1). Composite

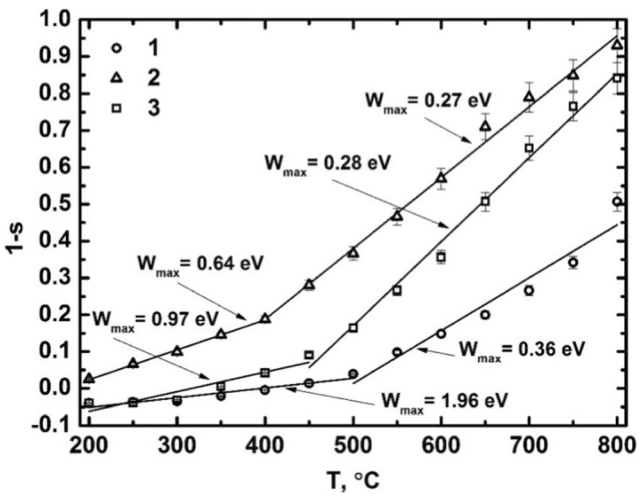

Fig. 7 Influence of the temperature on the (1 – s) parameter value for the ceramic composites based on PPT-7.5 (1), PPT-9.2 (2) and PPT-10.1 (3)

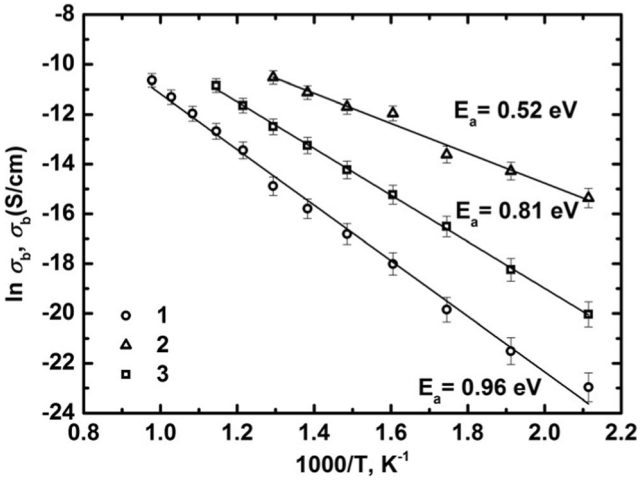

Fig. 8 Arrhenius plot of bulk conductivity for ceramic composites based on PPT-7.5 (1), PPT-9.2 (2) and PPT-10.1 (3)

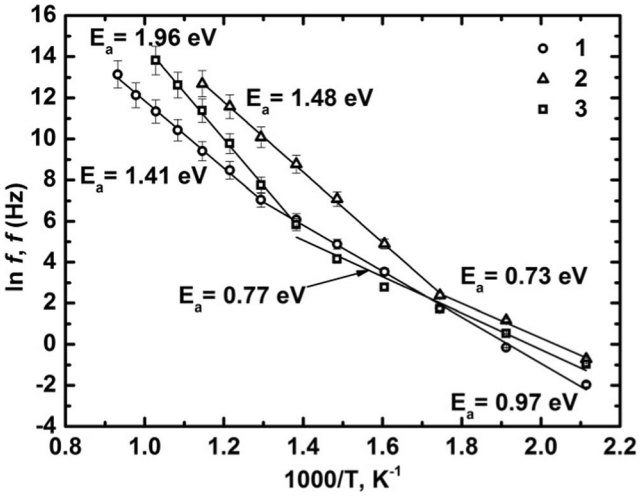

Fig. 10 Arrhenius plot of relaxation frequency calculated from Z"*(f)* for ceramic composites based on PPT-7.5 (1), PPT-9.2 (2) and PPT-10.1 (3)

based on potassium polytitanate with $[TiO_2]_0/[K_2O]_0 = 5.3$ has single-phase crystalline structure, consisting from $K_3Ti_8O_{17}$. Crystalline phase of $K_2Ti_4O_9$ in ceramics composition appears at ratio $[TiO_2]_0/[K_2O]_0$ of 7.1 in addition to $K_3Ti_8O_{17}$. The mixture of TiO_2 and $K_3Ti_8O_{17}$ phases is typical for the composite, characterized with $[TiO_2]_0/[K_2O]_0 = 11.7$.

The Z"-Z' dependence has two semicircles. Such behavior of curve indicates a presence of grain boundary and bulk structure effects in the electrical properties of this kind of ceramic composites [22, 23].

As seen from Tables 1 and 2, values of bulk and grain boundary parameters decrease with increasing the temperature. This phenomenon is typical for semiconductors characterized with a negative temperature coefficient of resistance (NTCR) [24–26].

In addition, it is observed the electrical conductivity increasing with the temperature growth. The composite based on potassium polytitanate with $[TiO_2]_0/[K_2O]_0 = 7.1$ showed the highest conductivity in comparison with other kinds of the obtained ceramics. σ_{dc} values of such ceramics are varied from $8{\cdot}10^{-10}$ S/cm to $6{\cdot}10^{-4}$ S/cm depending on temperature.

To explain the obtained results it is necessary to discuss the mechanism of the processes occurring in the investigated composites (Fig. 5). In the range of low frequencies, at all the temperatures, AC conductivity slightly increases with frequency due to polarization processes [27]; whereas, in the range of high frequencies, this parameter strongly increases with *f*. The last in the oxide ceramic materials usually is considered as a result of hopping charge transfer phenomenon [17]. The thermally activated character of the relaxation processes is confirmed by a shift of Z" and M" peaks towards higher frequencies with an increased temperature for all the composites (Tables 2 and 3) similar to the data reported in [28].

The processes of electrical charge transfer taking place at $T > 500$ °C can be considered taking into account that in

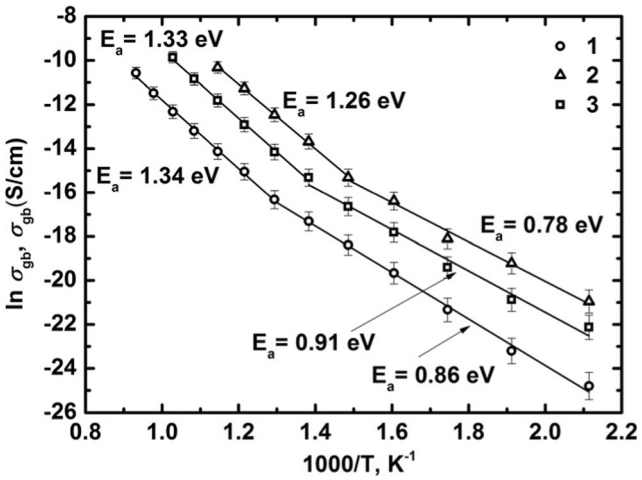

Fig. 9 Arrhenius plot of grain-boundary conductivity for ceramic composites based on PPT-7.5 (1), PPT-9.2 (2) and PPT-10.1 (3)

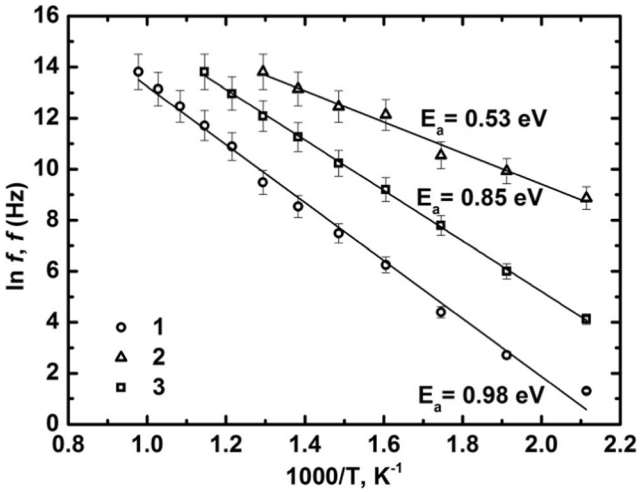

Fig. 11 Arrhenius plot of relaxation frequency calculated from M"*(f)* for ceramic composites based on PPT-7.5 (1), PPT-9.2 (2) and PPT-10.1 (3)

Table 4 The activation energy of DC conductivity, bulk and grain-boundary conductivity as well as relaxation frequency for ceramic composites based on potassium polytitanates obtained at different pH

pH	T, °C	Activation energy (E_a), eV				
		σ_{dc}	σ_{gb}	σ_b	f_{max} of Z”	f_{max} of M”
7.5	200–500	0.89 ± 0.10	0.86 ± 0.11	0.96 ± 0.05	0.97 ± 0.13	0.98 ± 0.09
	500–800	1.35 ± 0.12	1.34 ± 0.13		1.41 ± 0.21	
9.2	200–400	0.87 ± 0.11	0.78 ± 0.10	0.52 ± 0.04	0.73 ± 0.11	0.53 ± 0.05
	400–800	1.25 ± 0.15	1.26 ± 0.17		1.48 ± 0.15	
10.1	200–450	0.87 ± 0.09	0.91 ± 0.12	0.81 ± 0.08	0.77 ± 0.13	0.85 ± 0.06
	450–800	1.43 ± 0.25	1.33 ± 0.22		1.96 ± 0.23	

accordance with [12, 29, 30] for alkali titanate ceramic materials E_a (σ_{dc}, σ_{gb}, f_{max} of Z”) value depends on processes of charge carriers appearance and displacement over a long distance; while, E_a (σ_b, f_{max} of M”) value associates with migration of charge carriers (alkali ions) between the adjacent lattice sites. When, it is possible to assume that in the PPT based ceramic systems a value of E_a (σ_b, f_{max} of M”) is determined by polarization ability of K^+ ions located in the internal channels of crystalline potassium titanates. Some differences of their values recognized for different kinds of the investigated materials are caused by the character of structural defects represented in their bulk of grain [22].

On the other hand, the activation energy values of relaxation frequency obtained with the data on M” and bulk conductivity are very close to the E_a values of relaxation frequency determined from Z” and DC for grain boundary conductivity. Consequently, the charge carrier movement in grain bulk and grain boundary causes similar relaxation processes.

Two values of activation energy recognized for DC conductivity (Table 4, Figs. 6 and 9) indicate a presence of two mechanisms of the electric charge transfer processes, corresponding to different temperature ranges [31]. In accordance with [29, 31], relatively low activation energy values obtained for similar ceramic systems in the temperature range lower of 400–500 °C correspond to the electronic conductivity, while at higher temperatures, ionic conductivity can be considered as dominating process of the electric charge transport [29].

The comparison of our data on activation energy of electrical conductivity E_a (σ_{dc}, σ_{gb}, f_{max} of Z”) with the results obtained earlier for pure crystalline potassium titanates [5, 6, 32, 33] indicates that at $T < 400$ °C the investigated ceramic materials have E_a values very close to E_{dc} reported for the $K_2Ti_4O_9$ and $Na_2Ti_3O_7$ based ceramics. At the same time, at $T > 500$ °C the ceramic composites consisting of $K_2Ti_4O_9$ and $K_3Ti_8O_{17}$ have the E_a (σ_{dc}, σ_{gb}, f_{max} of Z”) values much higher of these ones mentioned in [5, 6, 32, 33]. This phenomenon can be attributed to more complicated character of grain boundary structure in the PPT based ceramic composites associated with a presence of several crystalline phases.

In accordance with [1, 34, 35], the activation energy values over 0.6 eV indicate formation of double ionized oxygen vacancies. Such reversible phenomenon takes place due to a presence of extrinsic lattice defect (Eq. 8 in Kröger–Vink notation). Furthermore, cation vacancies can be formed as a result of the irreversible processes of recombination with the electron of oxygen vacancy and partial potassium evaporation during the sintering (Eq. 9).

$$O_o^{\times} \rightleftharpoons V_O^{\bullet\bullet} + \frac{1}{2}O_2 + 2e \tag{8}$$

$$K_K = V_K^{''} + K + 2h \tag{9}$$

A negative charge appeared in the structure of the ceramic materials in accordance with Eq. 8 can migrate due to a hopping of electrons from Ti^{4+} to Ti^{3+}. The moving of potassium ions in the lattice of particles is a local parallel process to compensate the negative charge transfer. Thus, a presence of two types of conductivity (ion and electron), which is typical for similar oxide systems [36], can be proposed to consider the character of processes recognized in the ceramic materials obtained in this work.

In all the investigated composites at $T > 500$ °C E_a values for DC conductivity increase (Fig. 6). This fact allows proposing that at $T < 400$ °C the electric charge migration in the electric field is related to the double ionized oxygen vacancies formed as extrinsic lattice defects. Namely, the mixed ion-electron conductivity at the grain boundaries takes place due to formation of oxygen vacancies on the surface of PPT particles and causes increased electron density. At $T > 500$ °C an intensive formation of double ionized oxygen vacancies occurs in the grain bulk (intrinsic defects appearance). This process makes a significant contribution to the overall DC conductivity but has higher activation energy, in comparison with the formation of extrinsic lattice defects, supporting increased E_{dc} values. At the same time, a value of the potential barrier W_{max} estimated in frame of the correlated barrier hopping (CBH) model drastically decreases (Fig. 7), indicating fast migration of electrons in the conducting band of the solid.

The obtained results indicate that the PPT based ceramics can be used in manufacturing of different electronic devices taking into account some features of their thermal behavior. At T < 400 °C such ceramic semiconductors could be applied in manufacturing of ceramic semiconductor thermistors

characterized with stable NTCR value due to negative temperature coefficient of resistance (NTCR). At the same time, the dependence of the electrical properties of such materials on frequency allow to use them in manufacturing of sensitive elements of semiconductor gas sensors based on the impedance data analysis [37]. In addition, studied ceramic composites can be considered as promising in high temperature oxygen sensors working at T > 500 °C.

5 Conclusions

1. The phase composition of the ceramic composites produced using amorphous potassium polytitanates as raw materials depends on chemical composition of the precursor. At $[TiO_2]_0/[K_2O]_0 = 5.3$ the crystalline structure consists of $K_3Ti_8O_{17}$; an increase of the $[TiO_2]_0/[K_2O]_0$ up to 7.1 promotes appearance of $K_2Ti_4O_9$ and $K_3Ti_8O_{17}$, while the following growth of this parameter up to 11.0 supports obtaining the mixture of different crystalline forms of TiO_2 and $K_3Ti_8O_{17}$. All the obtained materials contain also the amorphous phase, which is most developed in the composite based on PPT-9.2 ($[TiO_2]_0/[K_2O]_0 = 7.1$).
2. An increase of the temperature promotes increased electric conductivity for all the materials investigated. The system based on $[TiO_2]_0/[K_2O]_0 = 7.1$ allows obtaining the ceramics characterized with the best electrical conductivity: DC-conductivity changing from $8 \cdot 10^{-10}$ S/cm (200 °C) up to $6 \cdot 10^{-4}$ S/cm (800 °C).
3. The activation energy values obtained from M"*(f)* dependence and from the data on bulk (bulk of grain) conductivity have similar magnitude indicating a presence of the same mechanism of relaxation processes, namely, polarization ability of K^+ ions located in the interlayer space.
4. The activation energy values calculated from Z" *(f)* and from the data on DC conductivity also are similar; this fact can be explained by the same mechanism of relaxation and charge carrier movement processes. An increase of the temperature higher than ~ 450 °C in the investigated ceramic composites promotes the increased values of activation energy for DC conductivity, grain-boundary conductivity and relaxation process determined from Z" *(f)* data, indicating a change of the mechanism of conductivity most likely related to the appearance of mixed ion-electron conductivity.
5. The AC conductivity within the structure of PPT-based ceramics can be described by the barrier hopping model. The potential barrier W_{max}, calculated in accordance with this model, decreases at the temperatures higher than ~ 450 °C presumably due to increased electron density in defect sites related to double ionized oxygen vacancies formation.
6. The obtained results indicate that the PPT based ceramics can be used in manufacturing of different electronic devices, namely semiconductor thermistors and sensitive elements of semiconductor gas sensors based on the impedance data analysis.

Acknowledgements This research was financially supported by Ministry of Education and Science of the Russian Federation (project 4.6197.2017/8.9).

References

1. Y. Lin, S. Fang, D. Su, K.S. Brinkman, F. Chen, Nat. Commun. A **6** (2015)
2. C.M. Wang, J.F. Wang, Appl. Phys. Lett. A **89**, 202905 (2006)
3. J. Suchanicz, Mater. Sci. Eng., B. A **55**, 114 (1998)
4. P. Adhikari, R. Mazumder, S. Abhinay, J. Electroceram. A **37**, 127 (2016)
5. S. Pal, S.D. Pandey, P. Chand, Solid State Commun. A **69**, 1203 (1989)
6. S. Kikkawa, F. Yasuda, M. Koizumi, Mater. Res. Bull. A **20**, 1221 (1985)
7. T. Sanchez Monjaras, A. Gorokhovsky, J.I. Escalante Garcia, J. Am. Ceram. Soc. A **91**, 3058 (2008)
8. H.C. Gulledge, Ind. Eng. Chem. A **52**, 117 (1960)
9. S.R. Tandon, S.D. Pandey, J. Phys. Chem. Solids. A **52**, 1101 (1991)
10. E.V. Tretyachenko, A.V. Gorokhovsky, G.Y. Yurkov, F.S. Fedorov, M.A. Vikulova, D.S. Kovaleva, E.E. Orozaliev, Particuology A **17**, 22 (2014)
11. V.G. Goffman, A.V. Gorokhovsky, N.V. Gorshkov, F.S. Fedorov, E.V. Tretychenko, A.V. Sevrugin, Data in Brief A **4**, 193 (2015)
12. V.G. Goffman, A.V. Gorokhovsky, M.M. Kompan, E.V. Tretyachenko, O.S. Telegina, A.V. Kovnev, F.S. Fedorov, J. Alloys Compd. A **615**, S526 (2014)
13. A.V. Gorokhovsky, E.V. Tretyachenko, V.G. Goffman, N.V. Gorshkov, F.S. Fedorov, A.V. Sevryugin, Inorg. Mater. A **52**, 587 (2016)
14. N. Bao, X. Feng, X. Lu, Z. Yang, J. Mater. Sci. A **37**, 3035 (2002)
15. Y. Park, K. Terasaki, K. Igarashi, T. Shimizu, Adv. Compos. Mater. A **10**, 17 (2001)
16. M.I. Biryukova, I.N. Burmistrov, G.Y. Yurkov, I.N. Mazov, A.A. Ashmarin, A.V. Gorokhovskii, V.I. Gryaznov, V.M. Buznik, Theor. Found. Chem. Eng. A **49**, 485 (2015)
17. N.F. Mott, E.A. Davis, *Electronic Processes in Non-Crystalline Materials* (Clarendon press, Oxford, 1971)
18. A.K. Jonscher, Nature A **267**, 673 (1977)
19. J.T. Gudmundsson, H.G. Svavarsson, S. Gudjonsson, H.P. Gislason, Physica B: Condens. Matter A **340**, 324 (2003)
20. U. Akgul, Z. Ergin, M. Sekerci, Y. Atici, Vacuum A **82**, 340 (2007)
21. G.E. Pike, Phys. Rev. B: Condens. Matter. A **6**, 1572 (1972)
22. R. Muccillo, E.N.S. Muccillo, J. Electroceram. A **38**, 24 (2017)
23. E. Barsoukov, J.R. Macdonald, *Impedance Spectroscopy Theory, Experiment, and Applications* (Wiley, Canada, 2005), pp. 129–204
24. A. Feteira, J. Am. Ceram. Soc. A **92**, 967 (2009)
25. J.T. Irvine, D.C. Sinclair, A.R. West, Adv. Mater. A **2**, 132 (1990)
26. L.L. Hench, J.K. West, *Principles of Electronic Ceramics* (Marcel Dekkar, New York, 1989)
27. A.V. Gorokhovskii, V.G. Goffman, N.V. Gorshkov, E.V. Tret'yachenko, O.S. Telegina, A.V. Sevryugin, Glass Ceram. A **72**, 54 (2015)
28. S. Sumi, P.P. Rao, P. Koshy, Ceram. Int. A **41**, 5992 (2015)

29. A. Molak, E. Ksepko, I. Gruszka, A. Ratuszna, M. Paluch, Z. Ujma, Solid State Ion. A **176**, 1439 (2005)
30. L. Liu, Y. Huang, C. Su, L. Fang, M. Wu, C. Hu, H. Fan, Appl. Phys. A. A **104**, 1047 (2011)
31. A.G. Krasnov, I.V. Piir, M.S. Koroleva, N.A. Sekushin, Y.I. Ryabkov, M.M. Piskaykina, V.A. Sadykov, E.M. Sadovskaya, V.V. Pelipenko, N.F. Eremeev, Solid State Ion. A **302**, 118 (2017)
32. R. Haase, *Thermodynamics of Irreversible Processes* (Addison-Wesley, Reading, 1962)
33. R. Hu, B.A. Cola, N. Haram, J.N. Barisci, S. Lee, S. Stoughton, G. Wallace, C. Too, M. Thomas, A. Gestos, M.E. dela Cruz, J.P. Ferraris, A.A. Zakhidov, R.H. Baughman, Nano Lett. A **10**, 838 (2010)
34. F.A. Kröger, H.J. Vink, J. Phys. Chem. Solids. A **5**, 208 (1958)
35. A.S. Bondarenko, G.A. Ragoisha, J. Solid State Electrochem. A **9**, 845 (2005)
36. G. Gregori, R. Merkle, J. Maier, Prog. Mater Sci. A **89**, 252 (2017)
37. F.S. Fedorov, A.S. Varezhnikov, I. Kiselev, V.V. Kolesnichenko, I.N. Burmistrov, M. Sommer, D. Fuchs, C. Kübel, A.V. Gorokhovsky, V.V. Sysoev, Anal. Chim. Acta A **897**, 81 (2015)